Applied Catalysis A: General 500 (2015) 40–50

Contents lists available at ScienceDirect

Applied Catalysis A: General

journal homepage: www.elsevier.com/locate/apcata

An improvement of photocatalytic activity of TiO_2 Degussa P25 powder

V.G. Bessergenev[a,*], M.C. Mateus[a], A.M. Botelho do Rego[b], M. Hantusch[c], E. Burkel[c]

[a] Universidade do Algarve, FCT, Campus de Gambelas, Faro 8005-117, Portugal
[b] CQFM and IN, Instituto Superior Técnico, Universidade de Lisboa, Lisboa 1049-001, Portugal
[c] University of Rostock, Institute of Physics, Rostock, Germany

ARTICLE INFO

Article history:
Received 28 January 2015
Received in revised form 29 April 2015
Accepted 3 May 2015
Available online 11 May 2015

Keywords:
Nano-powder
Titanium dioxide
Photocatalysis
Water treatment

ABSTRACT

The photocatalytic activities of Degussa P25 powders annealed at various temperatures in vacuum and air were studied together with investigations of their compositions by XPS, of their crystal structures by XRD and of their specific surface areas by BET. It is shown that the photocatalytic activity of P25 powders was remarkably enhanced after vacuum annealing; the kinetic coefficient can be raised by 75% during annealing at 400 °C. It is obvious that this enhancement is not related to the adhesion ability of the P25 powders.

1. Introduction

It is generally accepted that the theoretical model of photocatalysis on a TiO_2 surface consists of different consecutive steps, where each one is essential for the activity and the efficiency of the photocatalyst [1]. The initial step of the photocatalytic process consists in the generation of electron–hole pairs upon irradiation of the material with photons of energies that are at least equal to those of the band gap values. In the second step, the formed electron–hole pairs can either recombine in the bulk or diffuse to the surface where they can participate in chemical reactions. In this step, the lifetime and the velocity of the electron–hole recombination is crucial. Charge carrier traps are used to promote the trapping of electrons and holes at the surface leading to recombination suppressing and to more efficient charge transfer processes.

The next step is the creation of $H^{\bullet}$* and $OH^{\bullet}$* radicals as a result of the electron–hole interaction with water and, finally, a probable multiple step reaction of organic compounds with active radicals. The electron transfer process is more efficient if the species are pre-adsorbed on the surface [2]. However, so far, the influences of the different stages of this model on the final efficiency of the photocatalysts were not well determined.

It should be emphasized that the photocatalytic activity of TiO_2 depends on quite a number of parameters including the crystal structure, the ratio between the anatase and the rutile phases, the particle size, the specific surface area and the mean pore size [3]. In addition, TiO_2 is a material that is very adequate to build tiny structures in all sorts of sizes and shapes [4]. In particular, TiO_2 samples prepared and treated by different methods exhibit a great variety in photocatalytic efficiency even though they have the same crystal form. Beyond this, the kinetic constant of the photocatalytic degradation depends on the conditions of the experiment, namely, whether the heterogeneous catalysis is taking place on the solid/gas surface or on the solid/liquid one.

Using first-principles calculations, the total energies of the stoichiometric TiO_2 surfaces along with the equilibrium shapes (the Wulff construction) of macroscopic rutile TiO_2 crystals have been established [5]. It was shown that the (1 1 0) surface has the lowest surface energy and that (0 0 1) surface has the highest one. The respective calculations of the surface energetics and the shape reconstruction of macroscopic crystals for anatase TiO_2 were also effectuated [6,7]. Anatase (1 0 1) and (1 0 0) surfaces have the lowest energies of 0.44 and 0.53 J/m^2, respectively, and the (1 1 0) surface has the highest energy of 1.09 J/m^2 which are all higher than the rutile (1 1 0) surface energy of 0.31 J/m^2. As a consequence, some of these surfaces can be present in nano-crystalline materials. However, it should be taken into account, for comparison with experimental crystal shapes, that the Wulff construction gives the equilibrium crystal shape of macroscopic crystal and that the

* Corresponding author. Tel.: +351 289 800900x7614; fax: +351 289 800066.
E-mail address: vbess@ualg.pt (V.G. Bessergenev).

http://dx.doi.org/10.1016/j.apcata.2015.05.002
0926-860X/

calculations are strictly valid only at zero temperature. Most of the methods for nanocrystals synthesis do not present equilibrium thermodynamic conditions.

The bulk structures of reduced TiO_{2-x} crystals are quite complex with various types of defects such as oxygen vacancies, Ti^{3+} and Ti^{4+} interstitials and planar defects such as crystallographic shear planes (CSPs). The defect structure varies with oxygen deficiency and the question which type of defect is dominant in which region of oxygen deficiency is still a subject of studies [3].

There is a vast spectroscopic and chemical evidence for the presence of point defects in samples annealed in vacuum that leads to the presence of Ti^{3+} ions. Their concentration is typically reported as being of several percent. The ultraviolet photoemission spectroscopy (UPS) spectra of single-crystal surfaces contain a band gap feature at ~1 eV below the conducting band edge which has been interpreted in terms of occupied Ti 3d states [8].

Various attempts for improving the photocatalytic properties of TiO_2 by annealing the samples in air and/or in vacuum have been made. These attempts were based on different ideas. Some of the obtained results are discussed below. Before, it should be emphasized that TiO_2 nanopowders prepared by different methods can have not only different morphology and different surface chemical composition, but also different crystal compositions. For this reason, all the experimental results can be divided into two classes, namely, into results obtained with powders prepared by different methods [9–13] and into results obtained with P25 powders [14–17]. It should be emphasized that no studies of changes in surface chemical composition along with a thermal treatment were done in all the above mentioned experimental studies. The kind of heterogeneous catalysis used for photolysis experiment is also important.

The existence of anomalies in temperature dependence of dielectric constant in anatase thin films was experimentally established in [18]. These anomalies can be easily created by annealing in vacuum and be suppressed in low pressure of oxygen and, therefore, they are supposed to be connected with oxygen vacancies. It means that electronic charge distributions in the region around vacancies are not symmetrical so that additional dipole moments are present [18], which can favourably influence the electron–hole separation. This mechanism was not considered neither by theory nor in experiments. Therefore, the essential new feature in the present paper is the aim to create oxygen vacancies by annealing in vacuum and to compare the results with annealing in air. Since, the presence of various species adsorbed on the TiO_2 surface influences the photocatalytic activity and changes in the surface chemical composition during temperature treatment XPS measurements were performed. In addition, based on the fact that the phases of anatase and rutile of P25 contain separated nanocrystals and that a direct electron transport between rutile and anatase through the common boundary does not exist, it is possible to estimate changes in the photocatalytic activity of anatase phase, separately.

2. Materials and methods

2.1. Sample preparation

Samples were prepared using the Degussa P25 powder with a grain size of about 20 nm. One series of the samples was annealed in vacuum ($\sim 2.5 \times 10^{-5}$ mbar) at temperatures between 20 and 750 °C for 4 h. During annealing the samples were placed in titanium foil crucibles within a stainless steel furnace with a copper cylinder for temperature homogenization. As heaters, two halogen lamps (1 kW) were used. Another series of samples were prepared by annealing in air at the same temperatures for 4 h.

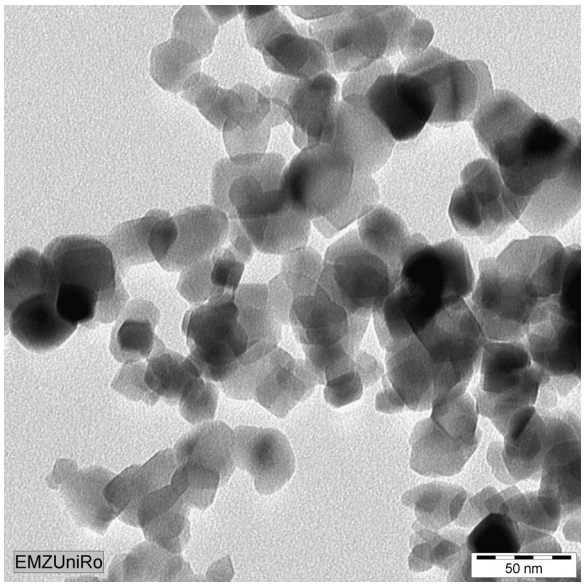

Fig. 1. TEM image of the Degussa P25 powder sample annealed at 200 °C, during 4 h.

In Fig. 1, a typical transmission electron microscopy (TEM) image of the sample annealed in vacuum at 200 °C is shown, evidencing that the grain sizes remained after annealing.

2.2. Phase control measurements

The crystal structure of the samples was studied using a high-resolution PANalytical x'PertPRO XRD instrument with Cu Kα radiation ($\lambda = 1.54184$ Å) in θ–2θ configuration. The anatase/rutile ratio in the samples was determined using Rietveld refinement procedure provided by FullProf program [19,20] as well as commercial PANalytical x'PertPRO software. For typical XRD pattern 2θ interval was 10–100° with the step $\Delta\theta = 0.008°$, the results of Rietveld refinement are shown in Fig. 2. The typical parameters of the refinement were $R_P \approx 5.4$, $R_{WP} \approx 7.81$, GOF–index ≤ 1.7.

2.3. XPS composition control

The TiO_2 samples were analyzed by X-ray photoelectron spectroscopy (XPS) using XSAM800 (KRATOS) X-ray spectrometer operated in the fixed analyser transmission (FAT) mode. An Al Kα (1486.7 eV) X-ray source was used. The analyser was operated at 20 eV pass energy both for detailed and survey spectra. All the binding energies were referenced to the C 1s peak at 285.0 eV, assigned to carbon singly bound to carbon and hydrogen. For quantification purposes, the following sensitivity factors were used: Ti 2p – 1.8, O 1s – 0.66 and C 1s – 0.25. Other details on data acquisition and treatment were as published elsewhere [21]. Some studies dedicated to the determination of the relation between Ti^{3+}/Ti^{4+} states for the samples annealed *in situ* in ultrahigh vacuum (10^{-9} mbar) were done using XPS setup with a PHI 5600ci spectrometer at the Leibniz Institut für Werkstoffkunde, Dresden. A monochromated Al Kα (1486.7 eV) X-ray source is used. The analyser operated at 5.85 eV pass energy for detailed spectra using a 0.05 eV step width. Calculation of the Ti^{3+}/Ti^{4+} concentration is based on the area ratio of these two titanium species in the $Ti2p_{3/2}$-peak.

2.4. Effective surface area measurement

To determine the specific surface area and the pore size distribution, a Micromeritics ASAP 2020–Physisorption Analyzer was

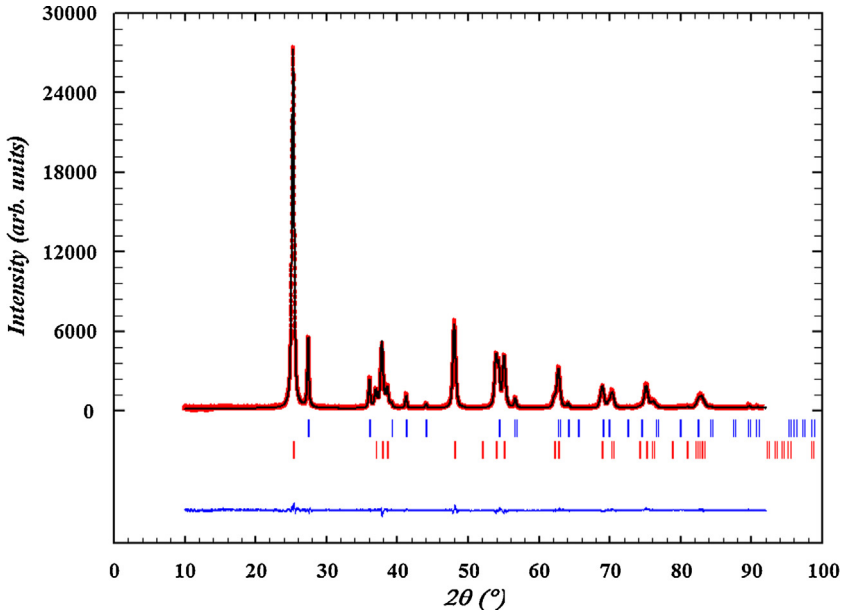

Fig. 2. Rietveld analysis of the X-ray powder diffraction from Degussa P25 sample annealed in vacuum at 400 °C during 4 h. The positions of the Bragg reflections are indicated by vertical bars (|). The difference between the experimental (dots) and the calculated (solid line) intensities from the refined model is shown by the plot in the lower part of the diagram (WinPLOTR – program of the FullProf suit).

used. Before the measurement, the samples were degassed at 50 °C for 10 h at a pressure of 50 mmHg. The weight of the sample was determined before and after the measurement. An isothermal adsorption of nitrogen was done at 77 K. The specific surface area is calculated by the BET equation in the range of $0.05 \leq p/p_0 \leq 0.25$. The pore size distributions and pore areas are derived by the Barret–Joyner–Halenda (BJH) analysis with Halsey corrections in the range of $0.42 \leq p/p_0 \leq 1$ of the adsorption branches for N_2 on the powders.

2.5. Photocatalytic activity measurements

The layout of the photoreactor apparatus was described in detail in [22]. Briefly, the volume of irradiated solution was of 7.9 ml with an optical thickness of 1 mm. A 200 W Xenon lamp was used as an UV light source and a water filter with fused silica windows was used in order to avoid an excessive heating of the solution. The photocatalytic process in water requires the presence of O_2 as electron acceptor; thus a continuous flow of air was injected by means of an air pump. Flow control was performed by stabilization of the same air pressure at the inlet of the photoreactor. Fenarimol (Riedel, 99.7%) 5 mg/l solutions were prepared in bidistilled water. The Fenarimol solution was left in contact with the reactor cell about 12 h in the dark before irradiation in order to achieve the adsorption equilibrium of the pesticide between the solution and the cell surfaces. During irradiation, 100 μl samples were taken every 0.25 h, and immediately analyzed on a HPLC system (Agilent Technologies 1220 LC Infinity system with UV detector) under the following experimental conditions: LichroCART 125-4 column: Lichrospher 100 RP-18, 5 μm; eluent: acetonitrile (Merck Lichrosolv) 65%, MilliQ water 35%; 1.0 ml/min flow; UV detection at 220 nm. The total irradiation time was between 1.5 and 3 h for each sample.

Two kinds of experiments were performed. It was noticed that the sedimentation rates were the same and that they were very slow for the samples annealed at temperatures 200–600 °C. However, for the samples annealed at even higher temperatures the sedimentation rates were drastically higher. The first kind of experiments was performed with powder samples dispersed in water solutions (10 mg/50 ml, for the samples with $T_{annealing} \leq 600$ °C). In order to be able to compare the reaction rates for all the samples, another type of experiment was performed. Hereby, samples with identical weight were deposited on fused silica substrates by evaporation from a TiO_2 aqueous suspension (10 mg/10 ml, the final amount of powder was determined by weighting after water evaporation) and tested under identical experimental conditions.

3. Results

In Table 1 the results of XRD and BET experiments for the samples annealed in vacuum and in air for 4 h are shown.

3.1. X-ray diffraction results

It can be seen from Table 1, that significant modifications of crystal structure and corresponding changes in anatase/rutile ratios take place for the samples annealed at temperatures higher than 550 °C. For the samples prepared at temperatures higher than 600 °C, there is also significant difference in the anatase/rutile ratio for the samples annealed in vacuum and in air, the data are shown in Fig. 3.

For the samples annealed in vacuum, the phase transformation from the anatase phase to the rutile phase occurs faster than for the samples annealed in air at the same temperatures. It can be supposed that surface oxygen defects, appearing during the sample annealing in vacuum, create more disordered surface states having lower potential barriers for atomic diffusion, thus allowing for faster phase transformations than in the case of sample annealing in air.

3.2. XPS surface composition control

The quantitative results of the surface compositions of the samples, annealed in air and in vacuum, obtained from XPS are presented in Table 2. Ti 2p spectra were fitted with a single peak assigned to Ti^{4+}. However, given the pronounced tail of the peak at lower binding energies (Ti $2p_{3/2}$) – a Gaussian–Lorentzian profile with around 80% Lorentzian contribution was needed to fit

Table 1
Rutile and anatase content in the samples annealed in vacuum and air from XRD data by Rietveld refinement analysis and corresponding surface and cumulative pore areas determined by BET experiments.

Annealing temperature (°C)	Rutile		Anatase		BET surface area (SA), m^2/g	Cumulative pore area (CA), m^2/g	Ratio CA/SA
	%, of fraction	Particle size, nm	%, of fraction	Particle size, nm			
Vacuum							
200	16.37	42.4	83.63	25.4	36.0	15.3	0.425
400	16.17	43.3	83.83	25.6	29.0	25.8	0.889
550	22.29	43.5	77.71	26.8	41.0	37.1	0.904
600	32.97	51.7	67.03	28.4	39.9	35.8	0.897
620	59.74	54.5	40.26	27.7	31.4	21.9	0.697
650	89.98	68.4	10.02	33.9	19.9	14.1	0.709
670	91.46	75.5	8.54	39.1	15.5	10.5	0.677
700	100	86.0	0	–	11.0	7.1	0.645
Air							
Not annealed	16.67	42.3	83.33	25.0	41.27	–	
200	16.53	42.6	83.47	25.2	55.5	44.1	0.794
400	16.57	44.5	83.43	25.7	57.2	41.0	0.717
550	21.78	48.5	78.22	28.6	44.9	32.9	0.733
600	32.29	50.0	67.71	28.4	38.2	31.4	0.822
620	46.58	61.0	53.43	32.6	29.8	30.2	1.013
650	63.41	66.5	36.59	32.4	22.3	19.9	0.892
670	77.03	75.9	22.97	35.2	20.3	19.4	0.956
700	93.44	97.8	6.56	45.8	13.3	11.6	0.872
750	99.2	119.6	0.8	–	–	–	

the spectra – we cannot discard the existence of a small contribution (around 2%) corresponding to Ti^{3+} species. Some important relations are also shown in Fig. 4(a–d).

As it can be seen from XPS data, the content of the structural oxygen (lattice O^{2-}) is, within the experimental error, the same for all temperatures of annealing giving the composition formula $TiO_{2.15 \pm 0.2}$ for the samples annealed in vacuum and $TiO_{2.10 \pm 0.11}$ for the samples annealed in air that corresponds to an experimental error of approximately 10%, taking into account that the information about the O^{2-} species is extracted from the fitted peak. It should be emphasized that the samples in XPS analysis present different anatase/rutile ratios. Up to-day, the equilibrium phase diagram for oxygen content in TiO_2 anatase and rutile phases at different temperatures in vacuum is still unknown. It is not obvious that, the changes in oxygen content in vacuum are the same, in these two phases. The obtained results show that those changes are smaller than 10%.

Essential decreases in carbon and non-structural oxygen contents are observed when the annealing temperature increases from 500 to 600 °C for both series of samples annealed in air and in

Table 2
XPS peaks intensities and relative contents obtained for the samples annealed in air and in vacuum.

$T_{annealing}$, °C	25	200	400	550	600	620	650	670	700	750	BE, eV	Assignment
Air												
Ti, $2p_{3/2}$	7.49	6.89	8.09	8.29	12.52	13.23	13.67	13.48	13.64	14.07	458.6	TiO_2
Ti, $2p_{1/2}$	3.44	3.28	4.05	3.99	5.98	6.37	7.41	7.99	7.26	7.38	464.2	
O1, 1s	24.78	22.85	24.82	26.57	39.04	38.90	41.03	42.28	43.76	45.83	529.7	O^{2-}, structural
O2, 1s	4.57	3.50	3.16	2.68	4.58	4.51	5.82	4.83	4.77	4.79	531.0	O, OH
O3, 1s	4.51	4.87	4.66	4.58	3.59	3.54	3.28	3.46	3.04	3.11	532.2	O=C
O4, 1s	1.96	3.01	2.56	2.95	1.29	1.18	0	0	0	0	533.5	H_2O, O–C
C1, 1s	41.24	44.97	44.38	42.14	27.98	26.60	24.26	21.49	24.80	21.69	285.0	C–C, C–H
C2, 1s	8.46	7.09	5.26	4.84	3.42	4.06	2.40	4.36	1.45	1.52	286.8	C–O
C3, 1s	3.55	3.54	3.01	3.96	1.59	1.60	1.92	2.11	1.27	1.61	289.0	O–C=O, CO_3
O/Ti	3.3	3.4	2.9	3.0	2.6	2.5	2.4	2.4	2.5	2.5		
O^{2-}/Ti	2.3	2.2	2.0	2.2	2.1	2.0	1.9	2.0	2.1	2.1		
C/Ti	4.9	5.5	4.3	4.1	1.8	1.6	1.4	1.3	1.3	1.2		
O(nO^{2-})/Cox	0.9	1.1	1.3	1.2	1.9	1.6	2.1	1.3	2.9	2.5		
Cox/Ctotal	0.2	0.2	0.20	0.2	0.2	0.2	0.2	0.2	0.1	0.1		
Vacuum												
Ti, $2p_{3/2}$		8.14	7.80	8.16	11.1	14.93	13.50	12.97	12.87		459.1	TiO_2
Ti, $2p_{1/2}$		4.26	3.73	4.01	5.70	7.67	6.39	6.93	6.18		464.8	
O1, 1s		26.49	26.15	26.36	36.90	45.22	43.24	40.82	41.54		529.7	O^{2-}, structural
O2, 1s		6.55	7.50	2.59	4.54	4.97	4.45	5.27	6.04		531.0	O, OH
O3, 1s		3.23	3.59	5.14	2.51	1.91	3.49	3.07	3.71		532.2	O=C
O4, 1s		0	0	2.54	0	0.64	0.72	0.81	0.46		533.5	O–C
O5, 1s		0	0	0.51	0	0.34	0.40	0.11	0.22		535.4	H_2O
C1, 1s		41.40	41.18	41.68	32.30	20.40	23.08	25.87	23.68		285.0	C–C, C–H
C2, 1s		6.84	7.20	5.52	4.98	2.47	3.08	2.57	3.38		286.4	C–O
C3, 1s		3.10	2.85	3.48	1.95	1.45	1.64	1.57	1.93		288.9	O–C=O
O/Ti		2.93	3.23	3.05	2.61	2.35	2.63	2.52	2.73			
O^{2-}/Ti		2.14	2.27	2.17	2.19	2.00	2.17	2.05	2.18			
C/Ti		4.14	4.44	4.17	2.33	1.08	1.40	1.51	1.52			
O(nO^{2-})/Cox		0.98	1.10	1.20	1.02	2.01	1.92	2.24	1.96			
Cox/Ctotal		0.19	0.20	0.18	0.18	0.16	0.17	0.14	0.18			

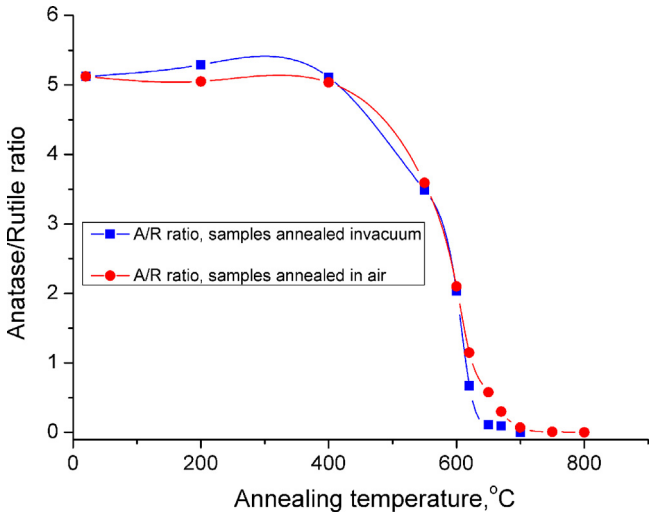

Fig. 3. Anatase/rutile ratio in dependence on annealing temperature in vacuum and in air.

vacuum. Also the oxidized carbon gets more strongly oxidized: (O non O^{2-})/C_{ox} changes from an average value around 1 till 550 °C to an average value around 2 from 600 °C on (Fig. 4a and c). These species of oxygen and carbon usually come from O^-, OH^-, H_2O, O–C absorbed on the surface or are obtained during the TiO_2 synthesis.

It can be accentuated that, after being annealed, the samples were exposed to air and did not return to the former content of these kinds of species. Common features in Fig. 4a and c are that the value O^{2-}/Ti remains constant and the value O/Ti (O – total oxygen content) decreases from 3 to 2.5 starting from 550 °C under annealing in air and in vacuum. Relative contents of various oxygen containing species obtained from oxygen peak by fitting, namely O1 (O^{2-}, structural), O2 (OH), O3 (O=C), O4, O5 (O-C, H_2O) are shown in Fig. 4b for the samples annealed in air and in Fig. 4d for the samples annealed in vacuum. It can be seen that temperature dependence of the $O1/O_{total}$ ratio is different for the samples annealed in air and in vacuum. The $O1/O_{total}$ ratio always increased upon annealing in air which means that both phases, anatase and rutile, gain some oxygen improving their stoichiometries, and that the $O1/O_{total}$ ratio decreased upon annealing in vacuum starting from 620 °C, where predominantly the rutile phase exists (see Table 1). The $O2/O_{total}$ ratio (O-O and O-H) has a complex behaviour upon annealing in air, but, taking into account the error of about 10%, it can be considered as approximately constant and in vacuum a decrease of this ratio is observed. The $O3/O_{total}$ ratio (O=C species) decreases in both cases and the (O4, O5)/O_{total} (H_2O, O-C species) ratio also decreases upon annealing in air and it is approximately zero in vacuum.

3.3. Specific BET surface area

An adsorption measurement exhibits several structural features. It is possible to conclude about the particle shape from the

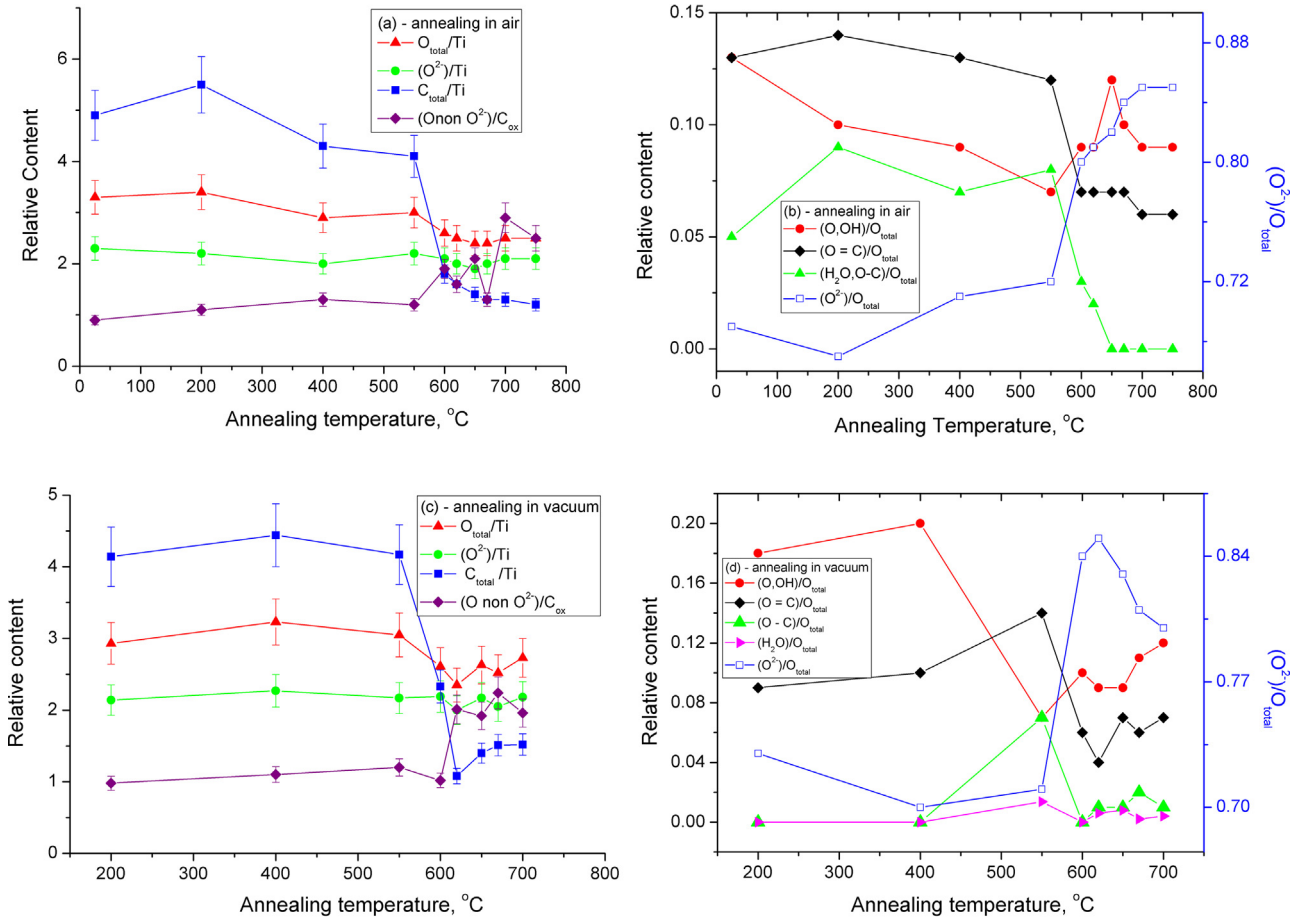

Fig. 4. (a) XPS atomic ratios O_{total}/Ti, O^{2-}/Ti, C_{total}/Ti, (O non O^{2-})/C obtained for the samples annealed in air. (b) XPS atomic ratios $O1/O_{total}$ (O1-O^{2-}), $O2/O_{total}$ (O2-O, OH), $O3/O_{total}$ (O3-O=C) and $O4/O_{total}$ (O4-H_2O, O-C) obtained for the samples annealed in air. (c) XPS atomic ratios O_{total}/Ti, O^{2-}/Ti, C_{total}/Ti, (O non O^{2-})/C obtained for the samples annealed in vacuum. (d) XPS atomic ratios $O1/O_{total}$ (O1-O^{2-}), $O2/O_{total}$ (O2-O, OH), $O3/O_{total}$ (O3-O=C) and (O4, O5)/O_{total} (O4-H_2O, O-C) obtained for the samples annealed in vacuum.

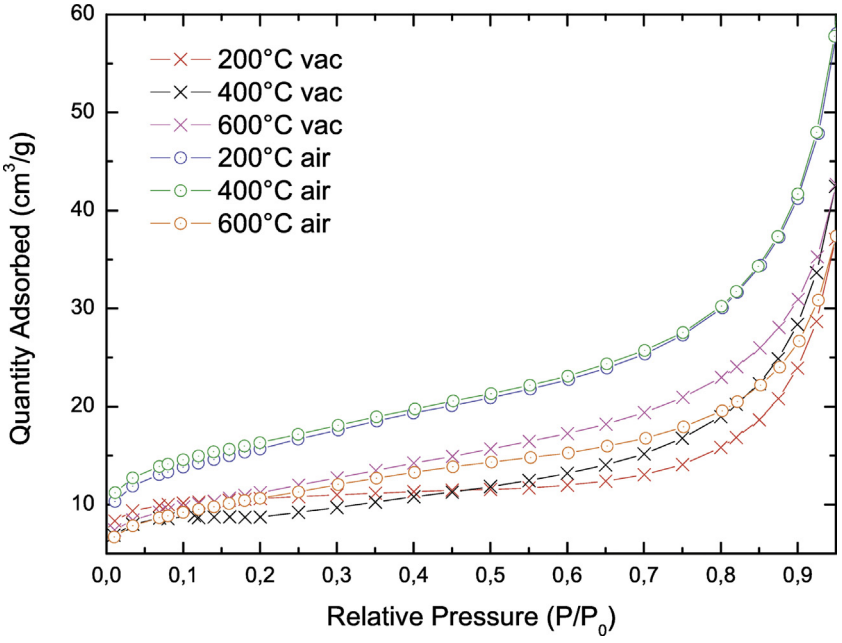

Fig. 5. Adsorption branches of N2-adsorption measurements at 77 K.

shape of the isotherm and the porous structure from the type of the hysteresis [23,24]. Each heat treated titania powder in this paper shows a type IV isotherm. The characteristics for the adsorption branch of this isotherm are shown in Fig. 5 and are similar to the isotherm type II.

A strong increase of adsorbed gas molecules is observed up to a relative pressure of $p/p_0 = 0.05$ where a monomolecular coverage is reached. The higher the quantity of adsorption at this point is, the bigger the specific surface area is. Typical adsorption branches are shown in Fig. 5.

At higher relative pressures, the adsorption branches present a small increase up to $p/p_0 = 0.7$. The slope of the curve depends on the mesoporous structure. In mesopores it is possible to build up a multimolecular coating while in micropores it is not possible. The curve for the powder treated at 600 °C in vacuum shows a bigger slope than the one treated at 200 °C in vacuum. The conclusion is that powders annealed at higher temperatures include more mesopores which is illustrated in Fig. 7.

At relative pressures near 1, structural information for the external surface area and macropores are included, since only for these structures a further adsorption is possible. The samples annealed at lower temperatures are showing a higher increase, so it is expected that the ratio of pore area and specific surface area is lower [23,24].

The differences between the isotherm types II and IV are in the desorption branch and are illustrated in Fig. 6. A hysteresis is detectable because of capillary condensation in the pores. The shape of the hysteresis determines the favourable shape of the pores and the end of the hysteresis, where the adsorption branch and the desorption branch are equal, determines the smallest

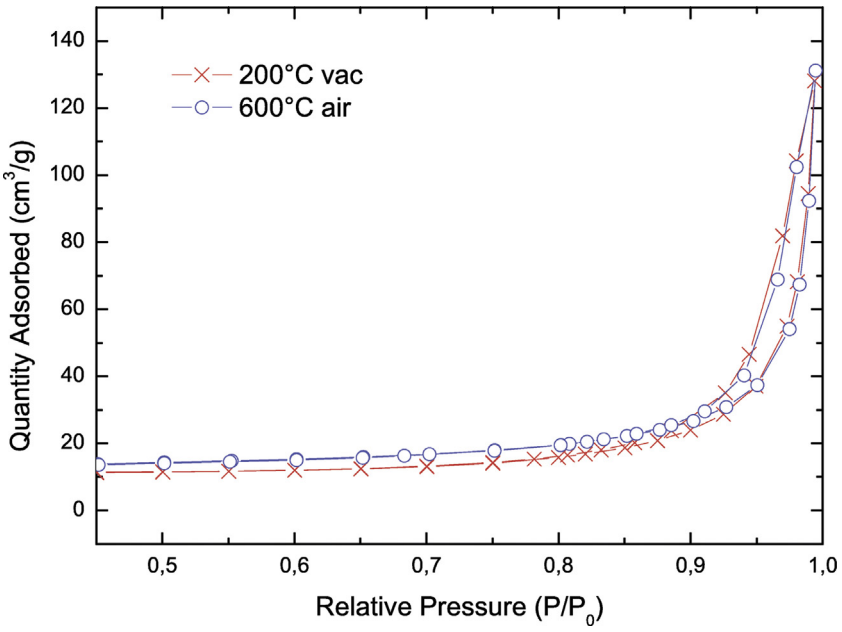

Fig. 6. Selected adsorption hysteresis of N2-adsorption at 77 K.

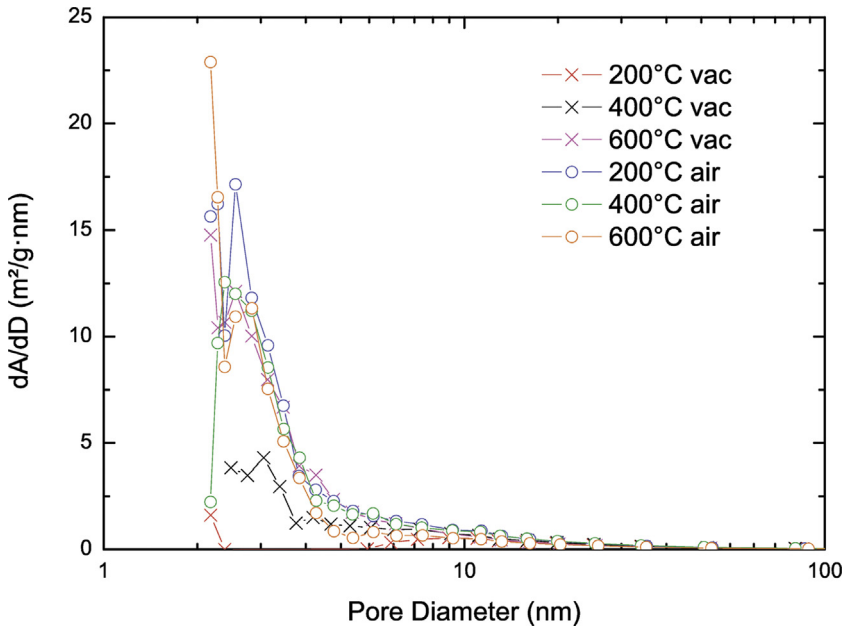

Fig. 7. Pore size distribution of selected samples.

diameter of the open pores. Because this point is at rather high relative pressures for each sample, it can be concluded that only the macropores are open pores while the mesopores are closed.

The combination of a type IV isotherm and a hysteresis type H3 for every sample leads to the fact that the powders aggregate to plate-like particles with slit shaped pores [23,24]. The calculated specific surface areas and pore areas are listed in Table 1.

The TiO_2 powders treated in air show a higher specific surface area in comparison with the samples annealed in vacuum, except, for the samples, treated at 600 and 620 °C. For these samples, specific surface areas are nearly equal. For samples treated in air, the ratio between the pore area and the specific surface area is increasing with raising the temperature from 400 up to 700 °C, whereas this ratio is decreasing for vacuum treated samples. Between 600 and 620 °C the mentioned ratio has the largest change for both atmospheres. This temperature range corresponds to a strong phase transition from anatase to rutile [25], as it can be seen in Table 1 and Fig. 3.

For vacuum annealed samples, a considerable increase in the specific surface area, observed at 550 and 600 °C, can be probably explained by vacuum cleaning of the surface because of evaporation of species containing carbon (see Fig. 4c). This effect of increase in the specific surface area for vacuum annealed samples was also observed in [16].

The pore size distribution, Fig. 7, shows a maximum of pores between 1.7 and 4 nm for every sample except for the 200 °C treated in vacuum. For this sample, no pores are detected in this size range. The air treated powders up to 600 °C contain a higher amount of detectable micropores, between 1.7 and 2.0 nm diameter, as well as mesopores.

The powder treated at 400 °C exhibits a small BET specific surface area under vacuum conditions and the largest one under normal air conditions, because of the mesoporous area. The evaporating or burning of organic rests or absorbed water in the powder produces cavities [23]. However, this requires oxygen in the atmosphere or high temperatures, which explains the differences in the pore size distribution of the 200 and 400 °C samples for both atmospheres. In the oxygen rich atmosphere, organic rests are burned out in the temperature range up to 300 °C, whereas an evaporation of these rests takes place in vacuum in a temperature range between 200 and 400 °C. Therefore, the air treated samples form a higher specific surface area due to a higher pore area compared to the samples treated in vacuum at lower temperatures.

As a consequence of the grain growth, pores are closed and the specific surface area as well as the pore area is decreasing. At higher temperatures, a new formation of pores is due to crystallization from amorphous material to anatase and re-crystallization, from anatase to rutile [26]. The higher amount of rutile in the vacuum treated powders combined with the smaller grain size implies that pore formation at temperatures around 600 °C is more favourable for these samples than for the air treated ones. This leads to the high amount of pores in the range from 4 to 10 nm for the 600 °C samples and the change in the mentioned ratio between the pore area and the specific BET surface area between 600 and 620 °C.

3.4. Photocatalytic activity

Table 3 shows the results of the study of the kinetics of Fenarimol photocatalytic degradation.

There are three different degradation processes that occur in the photocatalytic reactor simultaneously with very different kinetic constants. The first process is the degradation on the anatase phase surface of TiO_2 powder. This process has the highest kinetic constant. The second process is the degradation on the rutile phase surface with the kinetic constant much lower than that of anatase. Samples annealed in vacuum at temperatures equal to or higher than 700 °C have 100% of rutile phase and show such kinetic constants (see Table 3). The third process is the Fenarimol direct degradation by UV light in the reactor without TiO_2 powder which has the lowest kinetic constant. The kinetic constant of Fenarimol degradation can be calculated from the first order kinetic eq. (1):

$$\ln\left(\frac{I_t}{I_0}\right) = -k \times t \quad (1)$$

where I_t and I_0 are the current and initial HPLC chromatographic integrated peak intensities at 220 nm, k is the kinetic constant and t is time in hours. All three processes of degradation are independent on each other and, according with [17], there is no synergetic effect of co-presence of anatase and rutile on photocatalytic activity of P25, consequently, kinetic constant can be represented as a

Table 3
Photocatalytic activity of the samples annealed in vacuum and in air with two different function modes of the reactor: powder deposited on the glass and dispersed in the solution.

$T_{annealing}$, °C	Sample mass, mg	k, h^{-1}	k_A/g, $(h \times g)^{-1}$	Effective area, m^2/g	k_{AS}/m^2, $(h \times m^2)^{-1}$
Powder annealed in vacuum					
20	8.7	3.02	421	41.27	10.2
200	9.0	3.45	425	36.0	11.81
400	9.1	5.28	618	29.0	21.31
550	7.9	2.89	424	41.0	10.34
600	8.5	2.31	354	39.9	8.87
620	7.9	2.63	725	31.4	23.09
650	8.2	0.77	498	19.9	25.03
670	7.3	0.67	519	15.5	33.48
700	9.5	0.39	–	11.0	–
Direct degradation	0	0.26	–	–	–
Powder annealed in air					
20	8.7	3.02	421	41.27	10.2
200	8.0	2.57	343	55.5	6.18
400	8.4	2.58	327	57.2	5.72
550	7.6	2.74	414	44.9	9.22
600	8.5	2.43	370	38.2	9.69
620	7.9	2.57	505	29.8	16.95
650	9.2	2.14	536	22.3	24.04
670	8.0	0.87	288	20.3	14.19
700	7.4	0.55	394	13.3	29.62
Powder annealed in vacuum. Suspension					
20	10.0	0.891	69	41.27	1.67
200	10.0	0.838	62	36.0	1.72
400	10.0	1.039	86.1	29.0	2.97
600	10.0	0.725	52.1	39.9	1.31
700	10.0	0.350	–	13.3	–

sum of the constants $k = k_A + k_R + k_D$, where k_A, k_R are the constants for anatase and rutile phases and k_D is the constant of direct degradation. From Table 1 the fractions of the anatase and rutile phases can be determined for each sample annealed in vacuum or in air. By calculating specific kinetic constant for the rutile phase k_R/m, where m is the mass of the 100% rutile sample, it is possible to calculate the specific kinetic constant for the anatase phase, according to eq. (2):

$$k_A = \frac{k - (m_R \times k_R + k_D)}{m_A} \quad (2)$$

The specific kinetic constants normalized for the mass in dependence on annealing temperature are shown in Fig. 8.

As it can be seen from Table 3 the changes in specific area for the samples annealed in vacuum and in air at temperatures $T \leq 400$ °C are quite different. These samples, however, have the same anatase/rutile ratios (see Fig. 3 or Table 1) and consist mostly of the anatase phase (83%). Thus, the changes in the specific area can be attributed for anatase phase and the specific kinetic constants, normalized in respect of the area, can be calculated from Eq. (3). In support of this conclusion it can be mentioned that the specific areas for the samples annealed in vacuum and in air at 700 °C

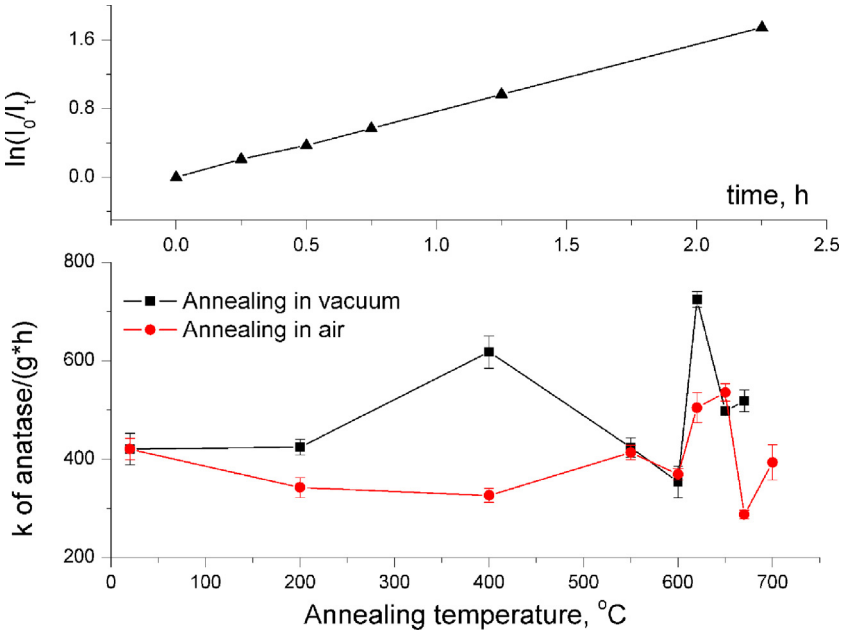

Fig. 8. Specific kinetic coefficient (k_A) of anatase phase calculated per unit mass. The graph of a typical kinetic curve, obtained for the sample annealed in vacuum at 650 °C is shown in the top part of the figure.

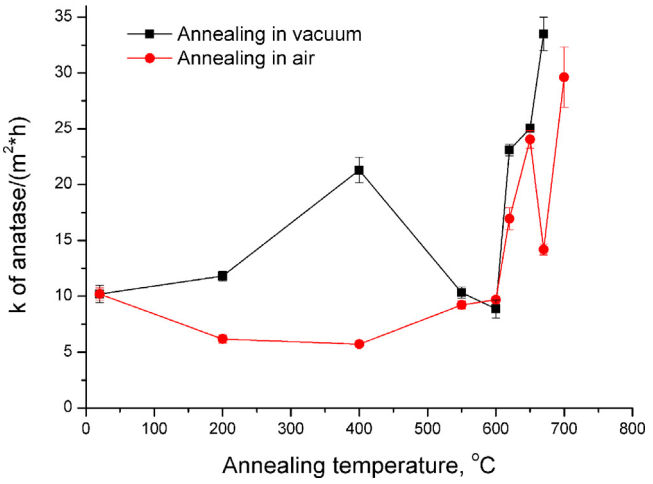

Fig. 9. Specific kinetic coefficient (k_{AS}) of anatase phase calculated per unit of specific area.

are almost the same (the sample annealed in air has small fraction (6.56%) of anatase).

$$k_{AS} = \frac{k_A}{\text{Specific area}} \quad (3)$$

The results are presented in Table 3 and in Fig. 9. They show that the samples annealed at 670 °C, both in vacuum and in air, have values of k_{AS} of about three times higher than the not annealed samples.

4. Discussion

There are a series of studies dedicated to the improvement of the photocatalytic properties of non-P25 samples prepared by different methods [9–13]. Generally, it was shown that by the method of heat treatment of these kinds of samples, in air or in vacuum, sometimes, the photocatalytic activity could be improved, however, no study succeeded to rise the photocatalytic activity significantly higher than that of the P25 powders.

Some works on commercial Degussa P25 TiO_2 powders can be mentioned, separately, because, as minimum, the initial materials have more or less the same characteristics in different studies.

It was found by Porter et al. [14] that annealing the P25 samples in air at temperatures from 600 to 1000 °C for 3 h significantly affects both the microstructure and the photoactivity. Over the range of calcination temperatures, the samples calcined at 650 °C revealed the highest photoactivities, which can be ascribed to an improvement in the crystallinity due to the calcination [14]. An increase in the photocatalytic activity for the sample calcined at 650 °C in comparison with the not treated P25 was found ~11.5% (data obtained from Table IV in [14]).

Yu et al. [15] studied P25 powder annealed in air and in vacuum at 200, 300, 400 and 500 °C for 3 h. A maximum in the photocatalytic activity was observed for the sample annealed at 400 °C in air. The increase in the photocatalytic activity in comparison to the vacuum treated sample at the same temperature was found to be about 32% (data obtained from Fig. 2 in [15]). This increase was attributed to the catalyst surface with more adsorbed oxygen that would generate more superoxide anion radicals under UV irradiation, resulting in a higher photoactivity [15].

The influence of the thermal treatment in air on the structure and the photocatalytic activity of TiO_2 P25 (P25 not treated, and annealed at 200, 300, 400, 500, 600 and 700 °C) was studied by Fernandes Machado and Santana [16]. The greatest activity for phenol degradation was obtained with untreated (original) TiO_2 P25 [16].

Recently, a crystalline composition of Degussa P25 powders was carefully studied along with the photocatalytic activity of artificially prepared powders obtained by mixing anatase, rutile and amorphous phases previously separated from P25 by selective dissolution [17]. It was found an existence of inhomogeneity of as-supplied P25 in the same package presumably because P25 is prepared by gas-flame synthesis; anatase, rutile and amorphous phases may be produced depending on flame conditions [17]. It was also found that the photocatalytic activity of the amorphous phase is negligible in comparison with the ones of the anatase and the rutile phases. It was also revealed that the components of P25, the anatase, the rutile and the amorphous phases behave independently without any interactions (absence of synergism) [17].

From this short description of theoretical and experimental results it can be concluded that: first, there is no evidence that nanoparticles, obtained by different procedures have the same relation between surfaces with different orientations (like in Wulff construction); second, an existence of additional electronic levels created by oxygen vacancies and situated at about 1 eV below the conducting band level is proved only for the rutile (1 1 0) surface; third, oxygen vacancies can be also created on the anatase phase surfaces but the energies for the creation of these vacancies are higher than that ones for the rutile surfaces. Experimentally, it was proven that the rutile surface has a lower photocatalytic activity than that one of the anatase phase, except in the cases when small metal clusters are present on the rutile surface [17]. The processes of the crystal structure formation (confirmed by XRD), the changes in the meso- and micropores distributions (confirmed by BET and BJH analysis) and the formation of oxygen vacancies and of Ti^{3+} and Ti^{4+} interstitials (confirmed by ESR) can affect the photocatalytic activities and all these factors contribute simultaneously.

As it follows from the obtained results of the present work, there are few important mechanisms that have strong influences on the photocatalytic activities.

First, it can be emphasized that, for the samples annealed at $T \leq 550$ °C in vacuum both configurations of the photocatalytic experiments—TiO_2 powder dispersed in solution and deposited on fused silica substrates gave the same results, namely an increase of the photocatalytic activity for the samples annealed at $T = 400$ °C in comparison with the samples annealed in air. At this temperature, there are neither significant changes in the anatase/rutile ratio (see Table 1) nor in the surface composition (see Fig. 4a–d). The difference between the surface areas for the samples annealed in air and in vacuum only increases the difference in k_{AS} values. Oxygen vacancies (or Ti^{3+} sites) have a strong influence on the dielectric constant [18] and on the electrical resistivity [27,28] and can be easily created at these temperatures by annealing in vacuum or by high-energy ball milling [29]. Recently Ti^{3+} surface defects, its properties, generation and photocatalytic application have been reviewed [30].

In this work P25 Degussa powders were annealed *in situ* in ultrahigh vacuum and respective XPS spectra of Ti were obtained after annealing. The regular increase in Ti^{3+}/Ti^{4+} ratio has been observed when temperature of annealing was increased. The values of Ti^{3+}/Ti^{4+} ratios changes from approximately 1.3% at room temperature (the sample was only placed into the chamber with ultrahigh vacuum without heating) to 1.38% at 200 °C and to 2.23% at 350 °C (the samples were heated at respective temperature under ultrahigh vacuum during 2 h). Despite the reducing atmosphere of around 10^{-9} mbar the amount of Ti^{3+} sites is very small. However, the pronounced tail the Ti $2p_{3/2}$ component in the low binding energy side (more visible than in the *ex situ* experiments),

strongly suggests the existence of the Ti^{3+} species even if its relative % is just of the order of 2%.

Second, when the temperature of annealing in vacuum increases from 550 to 600 °C, there are strong losses in the non-stoichiometric oxygen and surface carbon species, as it is shown in Fig. 4a and c. Adsorbed oxygen on TiO_2 surface scavenges the photo-induced electrons and inhibits the formation of Ti^{3+} sites [1]. Hence, when surface adsorbed oxygen and carbon containing species are removed, the process of the electron–hole recombination becomes more effective. This, in turn, results in decreasing the photocatalytic activity as it is shown in Fig. 8. As it can be also noted, the effective area at 550–600 °C (see Table 1) is almost equal for the samples annealed in vacuum and in air and the influence of changes in the effective area can be excluded at these temperatures.

Third, further increase in the annealing temperatures (T_{ann} > 600 °C) results in fast anatase to rutile phase transformations as it is shown in Fig. 3. The overall kinetic constant k decreases strongly at these temperatures because the rutile phase has lower photocatalytic activity. Nevertheless, at a temperature of 620 °C there is a critical increase in k_A as well as in k_{AS}. Unlike the 400 °C samples, this increase occurs in vacuum and in air treated powder. There are few processes taking place at the same time at T > 500 °C, namely: phase transformation, improvement of crystallinity (crystal growth) and oxygen vacancies formation. By the above described analysis it is possible to separate the effect of losses in the adsorption ability (decrease in specific surface area) from the electronic processes (hole action) and to show that the processes which depend on the electron–hole catalytic activity increase their efficiencies (k_{AS} growing upon annealing). In addition, the specific kinetic constant k_A does not change at 650 < T < 700 °C in vacuum and 670 < T < 700 °C in air because of two concurrent processes, namely, oxygen vacancies formation and losses in specific area (see Table 1 and Fig. 8). Contrarily, k_{AS} strongly increases in this temperature interval showing the efficiency of the induced electron trapping mechanism by Ti^{3+} sites (Fig. 9).

Fourth, as it can be seen from Fig. 7 and Table 1, the formation of pores is more effective during annealing in air than in vacuum. The size distribution of the pores is approximately the same in both cases. However, the photocatalytic activity, represented through the overall kinetic constant k and the specific constant k_A, of vacuum treated samples is higher than that of samples treated in air (for temperatures up to 600 °C). It means that the pores with sizes in the interval of 1.4–4 nm do not have significant influence on the photocatalytic activities of the TiO_2 powder samples.

There is some contradiction in the above mentioned literature about the existence [10] or non-existence [17] of synergism between the anatase and rutile phases. Additionally, Hurum et al. [31] observed the time dependence in the ESR signals coming from the rutile and anatase in aqueous P25 slurry after the UV illumination was switched off. In this time dependence, the ESR signal from the rutile phase was decreased and the signal from the anatase phase was increased at the same time. It was interpreted in terms of the existence of anatase electron trapping sites that can only be populated by electron transfer from the rutile to the anatase phase. Thus, according to the authors, the rutile phase acts as an antenna to improve the photoactivity [31]. However, in most of the cases, the anatase and rutile particles represent separate nanocrystals, so that the direct electron transfer across rutile/anatase border was not confirmed yet and there is no extension of the photoactivity into visible wavelengths. In [10], a particular case was considered, namely, relatively big rutile particles (small specific surface area) are photocatalytically active and covered by small anatase particles (big specific surface area). Therefore, an enhancement in the photocatalytic activity can arise from an adsorption ability of the anatase particles. In this work, it was confirmed that the pure rutile phase has a much lower activity than the anatase phase in a Fenarimol decomposition. Such effect was earlier observed for thin films for the samples with approximately the same surface area [32]. This gives an opportunity to estimate the photocatalytic activity of anatase phase separately.

5. Conclusions

Annealing of the Degussa P25 powders in vacuum and in air at different temperatures have been used to study the influence of oxygen vacancies on the photocatalytic activity of the samples. It was shown that the photocatalytic activity of the samples can be significantly increased by annealing in vacuum. The whole temperature interval of annealing between 25 and 750 °C should be divided into two zones: one zone up to 500 °C and another one higher than 500 °C. For T < 500 °C the increase in the photocatalytic activities for the samples annealed in vacuum (maximum at 400 °C) is independent on changes in the specific surface area. It can be explained by the ability of oxygen vacancies (or Ti^{3+} sites) to act as centres that prevent the electron–hole recombination and to increase the efficiency of the photocatalyst. It was also shown that oxygen and carbon containing species adsorbed on the surface or created in the Degussa technological process of synthesis of the powder play an important role in photocatalysis. Such a species scavenge photo-excited electrons and also prevent the recombination. When T > 500 °C, the processes of phase transformation, the crystal growth and the decrease in the specific surface area acts simultaneously. However, it was possible to show that the specific kinetic constant of the anatase phase (k_{AS}) increases with higher annealing temperatures. This means that the electron–hole mechanism of the decomposition of organics (Fenarimol) is still very effective.

Acknowledgements

The authors are grateful to Fundação para a Ciência e Tecnologia (FCT) Portugal for the financial support given in the framework of the development of scientific centres CIQA and CCMAR at Algarve University and to FCT project Pest-OE/CTM/LA0024/2013.

The authors are grateful to Prof. Martin Knupfer of the Leibnitz Institut für Werkstoffkunde, Dresden.

References

[1] A.I. Lisebigler, G. Lu, J.T. Yates Jr., Chem. Rev. 95 (1995) 735–758.
[2] R.W. Matthews, J. Catal. 113 (1988) 549–555.
[3] U. Diebold, Surf. Sci. Rep. 48 (2003) 53–229.
[4] A.N. Banerjee, Nanotech. Sci. Appl. 4 (2011) 35–65.
[5] M. Ramamoorthy, D. Vanderbilt, R.D. King-Smith, Phys. Rev. B 49 (1994) 16721.
[6] M. Lazzeri, A. Vittadini, A. Selloni, Phys. Rev. B 63 (2001) 155409.
[7] M. Lazzeri, A. Vittadini, A. Selloni, Phys. Rev. B 65 (2002) 199901.
[8] M.V. Ganduglia-Pirovano, A. Hofmann, J. Sauer, Surf. Sci. Rep. 62 (2007) 219–270.
[9] R.R. Bacsa, J. Kiwi, Appl. Catal. B 16 (1998) 19–29.
[10] T. Ohno, K. Tokieda, S. Higashida, M. Matsumura, Appl. Catal. A 244 (2003) 383–391.
[11] S. Bakardjieva, J. Šubrt, V. Štengl, M.J. Dianez, M.J. Sayagues, Appl. Catal. B 58 (2005) 193–202.
[12] K. Suriye, P. Praserthdam, B. Jongsomjit, Appl. Surf. Sci. 53 (2007) 3849–3855.
[13] T. Xia, Y. Zhang, J. Murowchick, X. Chen, Catal. Today 225 (2014) 2–9.
[14] J.F. Porter, Yu-G. Li, C.K. Chan, J. Mater. Sci. 34 (1999) 1523–1531.
[15] J.C. Yu, J. Lin, D. Lo, S.K. Lam, Langmuir 16 (2000) 7304–7308.
[16] N.R.C. Fernandes Machado, V.S. Santana, Catal. Today 107–108 (2005) 595–601.
[17] B. Ohtani, O.O. Prieto-Mahaney, D. Li, R. Abe, J. Photochem. Photobiol. A 216 (2010) 179–182.
[18] V. Bessergenev, Mater. Res. Bull. 44 (2009) 1722–1728.
[19] J. Rodriguez-Carvajal, An introduction to the program FullProf 2000, Laboratorie Léon Brillouin (CEA–CNRS) CEA/Saclay, France.
[20] L.B. McCusker, R.B. Von Dreele, D.E. Cox, D. Louer, P. Scardi, J. Appl. Crystallogr. 32 (1999) 36–50.

[21] A. Garbout, S. Bouattor, A.M. Botelho do Rego, A.M. Ferraria, A.W. Kolsi, J. Cryst. Growth 304 (2007) 374–382.
[22] V.G. Bessergenev, R.J.F. Pereira, M.C. Mateus, I.V. Khmelinskii, E. Burkel, R.C. Nicula, Int. J. Photoenergy 5 (2003) 99–105.
[23] G. Leofanti, M. Padovan, G. Tozzola, B. Venturelli, Catal. Today 41 (1998) 207–219.
[24] Kenneth Sing, Colloid. Surf. A 187 (2001) 3–9.
[25] C. Charles, A. Sorrell Dorian, H. Hanaor, J. Mater. Sci. 46 (2011) 855–874.
[26] K. Meyer, P. Lorenz, B. Böhl-Kuhn, P. Klobes, Cryst. Res. Technol. 29 (1994) 903–930.
[27] B. Huber, H. Gnaser, C. Ziegler, Surf. Sci. 566–568 (2004) 419.
[28] R. Amade, P. Heitjans, S. Indris, M. Finger, A. Haeger, D. Hess, Phys. Chem. Chem. Phys. 8 (2006) 777–782.
[29] R. Amade, P. Heitjans, S. Indris, M. Finger, A. Haeger, D. Hesse, J. Photochem. Photobiol. A 207 (2009) 231–235.
[30] L.-B. Xiong, J.-L. Lin, B. Yang, Y. Yu, J. Nanomater. 2012 (2012) 1–13.
[31] D.C. Hurum, A.G. Agrios, K.A. Gray, J. Phys. Chem. B 107 (2003) 4545–4549.
[32] V.G. Bessergenev, R.J.F. Pereira, M.C. Mateus, I.V. Khmelinskii, D.A. Vasconcelos, R. Nicula, E. Burkel, A.M. Botelho do Rego, A.I. Saprykin, Thin Solid Films 503 (2006) 29–30.